Mass Resolution Study in $S \to Z_d Z_d \to 4e$ Long-Lived Dark Photons Search & Front End Board Upgrades for the ATLAS Liquid Argon Calorimeter

Connor Stewart[1]

[1]Columbia University

August 1, 2025

Abstract

This report first covers a mass resolution study performed in the search of long-lived kinetically mixed dark photons which are new spin-1 bosons Z_d (with a mass between 10 and 290 GeV) that decay in the $S \to Z_d Z_d \to 4e$ mechanism from a new scalar boson S (with a mass between 60 and 600 GeV). The study identifies trends in the resolution (σ of a gaussian fit) of mass histograms both in events with 2 DV-matched electrons per displaced vertex and with no matched electrons using Monte Carlo signal simulations of proton-proton collisions in the LHC ATLAS detector with $\sqrt{s} = 13.6$ TeV. The following section covers an analysis of the calibration constants collected from the COLUTA ADC ASIC chip components of existing prototype FEB2 boards in preparation for the development of quality control checks on future boards which will be implemented into the upgraded High Luminosity LHC. The analysis identifies chips with significant outliers to observe if the corresponding boards perform abnormally in testing.

Contents

1 Introduction

1.1 The Standard Model and Beyond

Building off of decades of particle physics research, physicists developed the Standard Model (SM) in the 1970s as a framework to describe the fundamental components and interactions in the world. The SM has since become a robust and well-tested formulation that accurately predicts much of the observed phenomena seen in experiments [1].

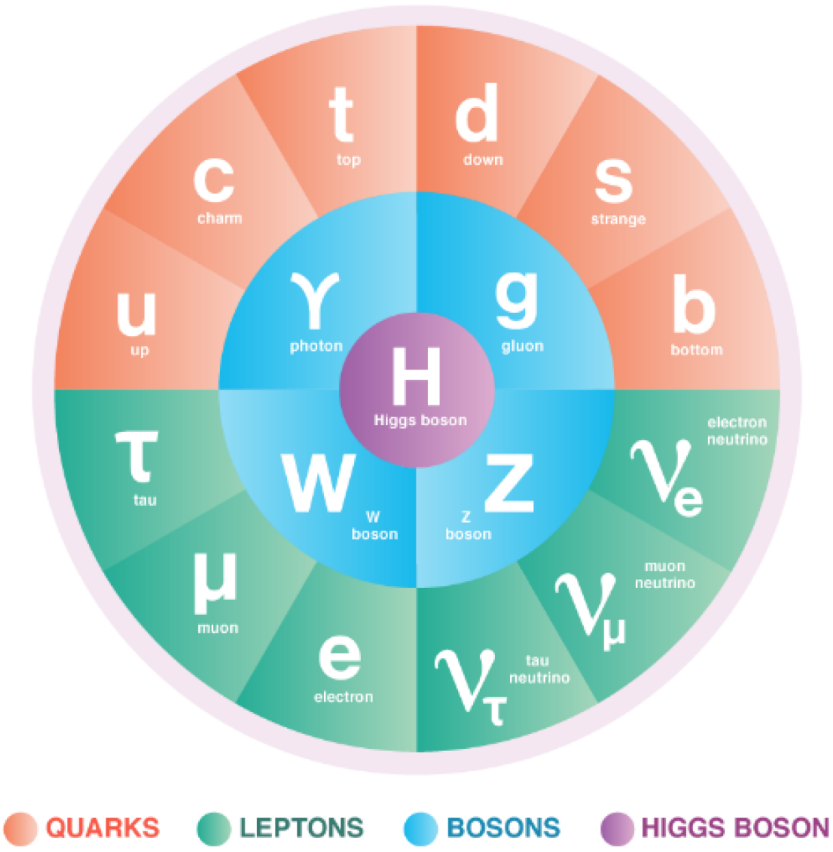

Figure 1: *A diagram of the SM, with fermions in the outermost ring showcasing quarks in orange and leptons in green, gauge bosons in blue in the middle ring, and the Higgs boson in the center in purple [2].*

The SM lists the fundamental particles of the universe, which it divides between classes called fermions and bosons. Fermions are the fundamental particles which make up all matter, which themselves are divided between quarks and leptons. Both of these groups contain three pairs of particles, known as generations, which are ordered from lightest to heaviest. The first generation of quarks is made up of the up and down quarks, the second generation made up of the charm and strange quarks, and the third made up of the top and bottom. Similarly, the generations of leptons are the electron, muon, and tau paired with their respective neutrinos. The first generations are the most stable, and make up all stable composite matter in the universe, with matter made up of the second and third generation fermions decaying into more stable forms.

The second type of particle described by the SM is the boson. Bosons are force carrier particles associated with the fundamental forces. The four fundamental forces are the electromagnetic (EM) force, the weak force, the strong force, and gravity. Of the bosons, the photon mediates the EM force, the gluon mediates the strong force, and the $W^{\pm}$ and Z^0 bosons mediate the weak force. The SM currently does not account for gravity, with some theories proposing a hypothetical graviton as the boson which mediates it. The last boson described by the SM is the Higgs boson, a result

of the Higgs field which gives particles their mass through the Higgs mechanism. Whereas the other four bosons are all of spin 1, the Higgs boson is a scalar boson with spin 0.

The SM has been extensively tested over the course of many years and has proven to match experiment very closely, with it successfully having predicted the existence of quarks, the $W^{\pm}$ and Z^0 bosons, and the Higgs boson. However, it's still notably incomplete. In addition to gravity, there are things the SM does not yet account for such as what happened to matter after the Big Bang, and in particular dark matter. Physicists have observed galaxies rotating at a speed which is thought to be impossible with the amount of observed mass they have without breaking apart. Thus it is believed there exists dark matter which does not interact with the EM force and makes up around 27% of the universe [3]. Therefore finding this dark matter is a primary goal of many experiments in Beyond the SM (BSM) physics.

1.2 Instrumentation

1.2.1 The Large Hadron Collider

In 2008 the European Council for Nuclear Research (CERN) first started up the Large Hadron Collider (LHC), the world's highest energy particle collider, which was build in the tunnels previously occupied by CERN's Large Electron-Positron Collider under the Swiss-French border in Geneva, Switzerland. The tunnels housing the LHC are around 27 kilometers long and it connects to several other accelerators operated by CERN, which are needed to reach the LHC's collision energy of up to $\sqrt{s} = 14$ TeV, an energy high enough to study many possible BSM phenomena.

To achieve proton-proton collisions at this energy, electrons are stripped away from Hydrogen atoms and the remaining protons are accelerated to 50 MeV by CERN's linear accelerator (LINAC). It is then similarly accelerated by the Proton Synchrotron Booster (PSB), the Proton Synchrotron (PS), and the Super Proton Synchrotron (SPS) to around 450 GeV, before finally entering the LHC itself in which the proton beam reaches over 7 TeV. Inside the LHC, radio frequency waves are used to accelerate the protons while superconducting magnets shape the beam along the path of the accelerator [4].

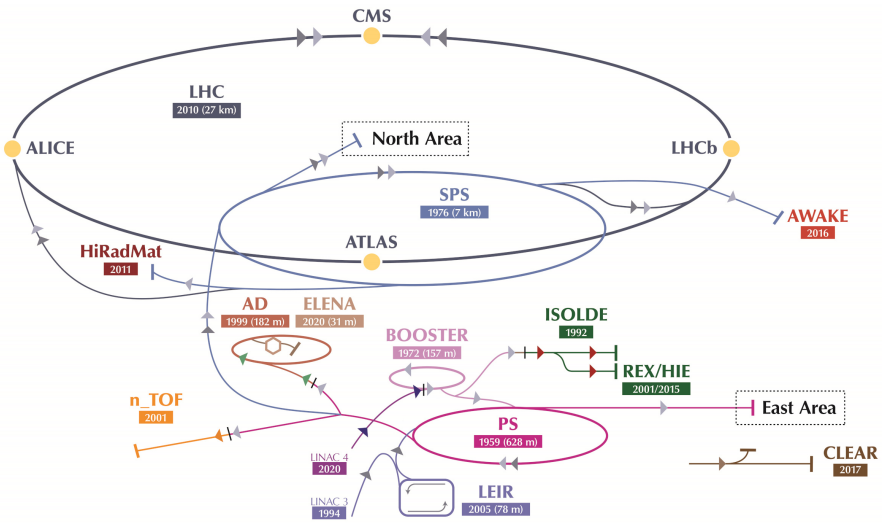

Figure 2: *The CERN accelerator complex, and injector chain of the LHC [5].*

1.2.2 The ATLAS Detector

There are multiple experiments run at CERN which have different detectors at various beam collision points along the LHC. These detectors track and reconstruct the collisions that occur to use for analysis. These include CMS, ALICE, LHCb, and notably A Toroidal LHC ApparatuS (ATLAS), which is one of two general purpose accelerators at the LHC.

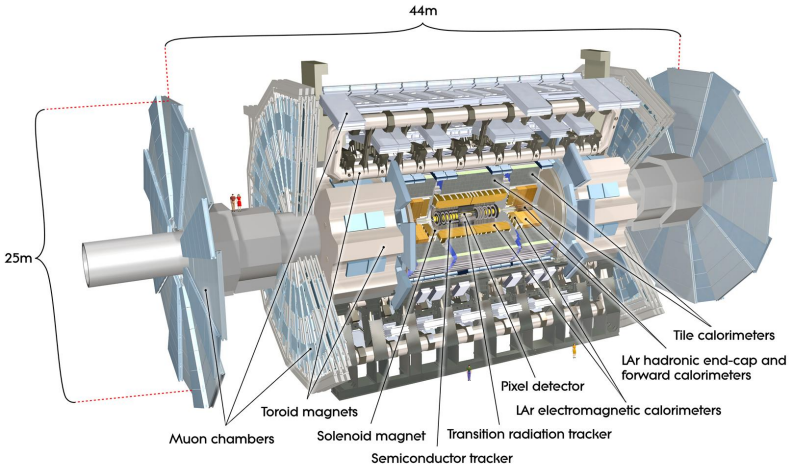

Figure 3: *The ATLAS detector [6].*

The ATLAS detector is comprised of three layers, the first of which is the Inner Detector (ID). The ID uses a magnetic field to bend charged particles in order to collect vertexing information on their tracks, as well as to measure the charge, momentum, and direction of the particles. The second layer contains the detector's calorimeters, which measure the energies of the particles that enter. The two calorimeters that make up this layer are the EM calorimeter and the hadronic calorimeter, which measure the energy of particles that interact electromagnetically and via the strong force respectively. They do this by measuring the currents from liquid argon (LAr) that absorbs incoming particles and becomes ionized. The last layer of the detector is the muon spectrometer which collects information on the tracks and momenta of muons which pass through the inner two layers of the detector.

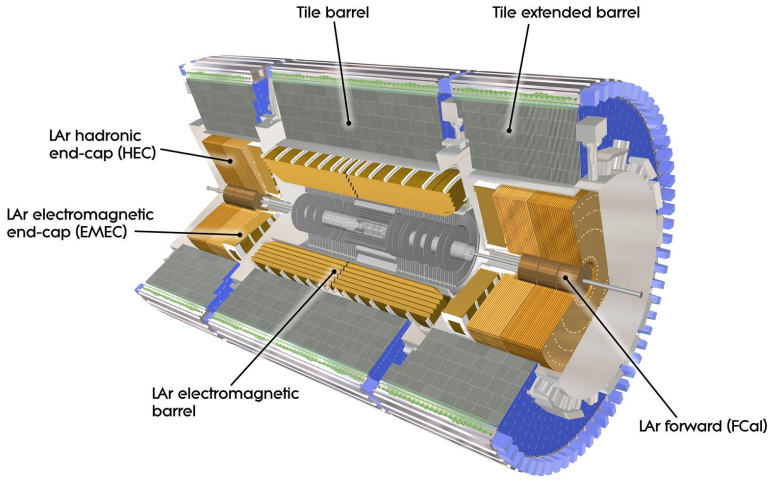

Figure 4: *The ATLAS LAr Calorimeter [7].*

The detector is over 46 meters long, weighs over 7000 tons, and sees over 1 billion collisions per second, making it an extraordinary resource with which physicists can study the physics that occurs at high energies, including many possible BSM phenomena [8].

2 $S \to Z_d Z_d \to 4e$ Long-Lived Dark Photons Search

2.1 The Hidden Abelian Higgs Model and Dark Photons

In a field theory, a gauge symmetry is a mathematical construct which informs how to transform elements of a field while keeping its observable properties the same. This involves performing a gauge transformation both on the elements of the matter field and a corresponding gauge field. These gauge transformations are the elements of the gauge symmetry.

In SM electromagnetism with the matter field ψ and gauge field $\mathbf{A}$ being the electron wavefunction and the vector potential respectively, their gauge symmetry is the $U(1)$ group, or the unitary group which contains all 1×1 unitary matrices, or in other words is (isomorphic to) the unit circle $\{e^{i\theta} : \theta \in \mathbb{R}\}$. To transform $\psi(x)$ while keeping the observables of the system the same, the gauge transformation must be an element of $U(1)$, forming group actions of $U(1)$ on $\psi(x)$ and on $\mathbf{A}$. When the gauge field $\mathbf{A}$ is quantized and excited, such as when the electron ψ corresponds to drops down its energy level, a photon is produced, which is the gauge boson for the electromagnetic force.

The SM gauge symmetry is $SU_C(3) \times SU_L(2) \times U_Y(1)$, the terms of which correspond to the strong, weak, and electromagnetic forces respectively, with their gauge bosons being the bosons that mediate those forces. The Hidden Abelian Higgs Model (HAHM) is one dark matter theory which proposes an additional "hidden sector" $U_D(1)$ gauge theory which is spontaneously broken, meaning the ground state of its matter field is no longer invariant under its gauge transformations. Much like how the SM photon is the gauge boson of the EM $U_Y(1)$ gauge symmetry, this theory is mediated by a new gauge boson Z_d, and also introduces a new Higgs-like scalar boson S, which can decay via $S \to Z_d Z_d \to 4e$ [9].

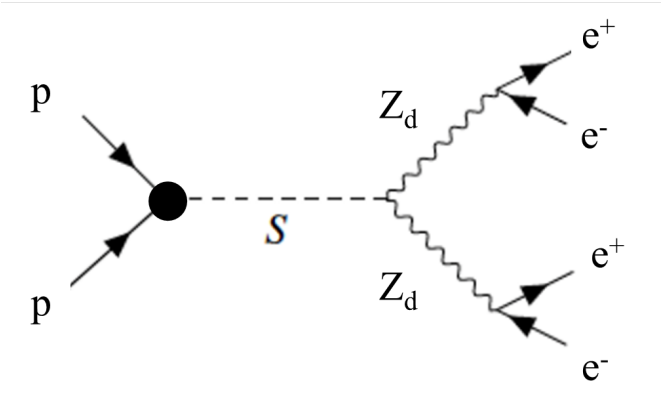

Figure 5: *Feynman diagram for the $pp \to S \to Z_d Z_d \to 4e$ decay process.*

This theory leaves the dark photon mass mZ_d, scalar mass mS, and dark photon lifetime τ as parameters, requiring analyses to account for different possible combinations of each.

2.2 Prompt Dark Photons Search

A search for prompt dark photons, meaning dark photons with lifetimes on a scale of less than picoseconds, has already been conducted by the ATLAS Collaboration. In this study, the study used Monte Carlo simulations of proton-proton collisions in the LHC to estimate the expected SM background which would appear behind a dark photon signal. The study then compared this background to data collected from the ATLAS detector in order to observe whether or not there appeared to be signals in excess of this which could suggest new physics or dark photons [10].

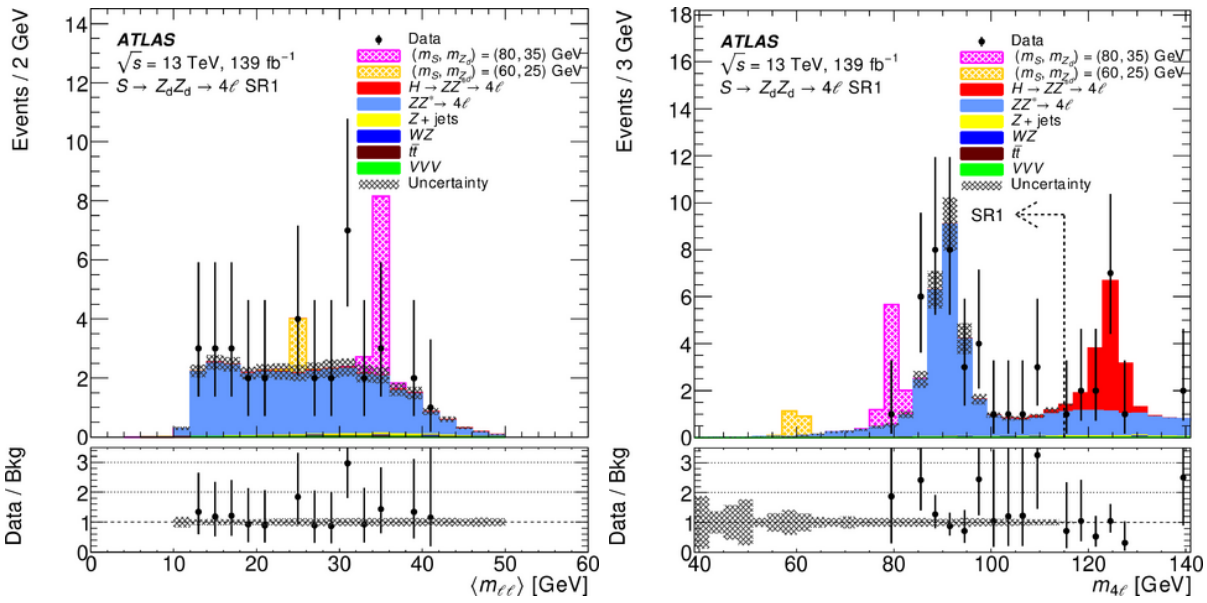

Figure 6: *The results of the search for prompt dark photons. Left: A plot of data (black dots) overlaid on simulated background (filled-in histograms) for $m_{\ell\ell}$, the proxy for mZ_d, showing a slight excess at 30 GeV. Right: A plot of data overlaid on simulated background for $m_{4\ell}$, the proxy for mS, showing a slight excess at 110 GeV [10].*

The results of the study were found to be in agreement with the SM and set limits on where future dark photon searches may be able to investigate. Among these results, the study observed a small excess of 1.6σ around $mS = 110$ GeV and $mZ_d = 30$ GeV. Thus the current search for long-lived dark photons allows for a closer look at this mass point to determine if the excess is a sign of new physics.

2.3 Long-Lived Dark Photons Search

The current search being conducted is for long-lived dark photons which have lifetimes on the scale of picoseconds and nanoseconds, which is possible if the coupling of the dark photons with the SM is small. The search is being conducted for mS between 60 and 600 GeV, mZ_d between 10 and 290 GeV, and with possible lifetimes at 0.1, 0.5, 2, and 10 nanoseconds. The motivation behind the search is the possibility that dark photons with a larger lifetime like these are capable of traveling further away from the primary collision point vertex before decaying at a displaced vertex (DV) into the final state, resulting in displaced electrons which could have eluded the limits of the prompt search. Thus it is an opportunity to further test the theory beyond the prompt search, as well as to investigate the small excess seen in it. Another impact of the displaced final state electrons is that the search only requires a two electron final state rather than four.

In order to analyze these displaced electron final states, they are tracked back to reconstructed displaced vertices. A displaced vertex is a point far away from the primary vertex where reconstructed particle tracks meet. The long-lived search looks for DV-matched electrons, which are electrons whose tracks are traced back to a reconstructed DV. The number of reconstructed electrons matched to a DV greatly impacts its reconstructed mass, and thus the analysis must focus separately on the cases where there are two, one, or no matched electrons.

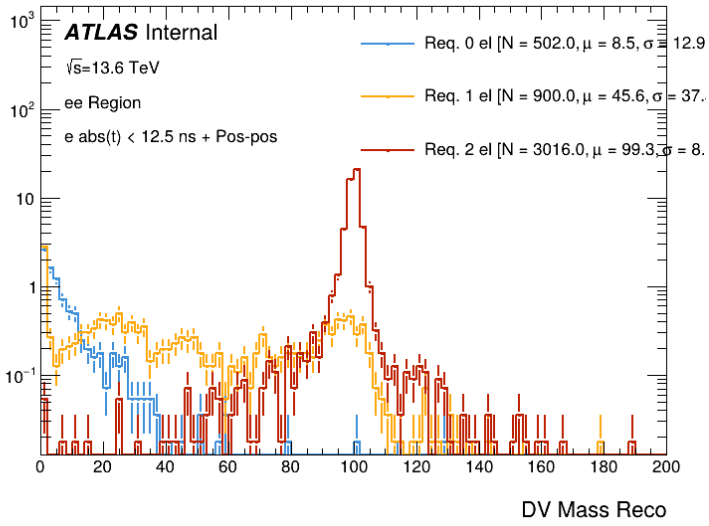

Figure 7: *Reconstructed DV mass histogram distributions for 0 (blue), 1 (orange), and 2 (red) DV-matched electrons per DV overlaid, with the clearest distribution visible in the 2 matched electron case.*

The analysis being performed by the group at Columbia focuses on the *ee* channel, which looks at final states comprised of DV-matched electrons in order to find potential DVs that represent dark photons decaying into two electrons.

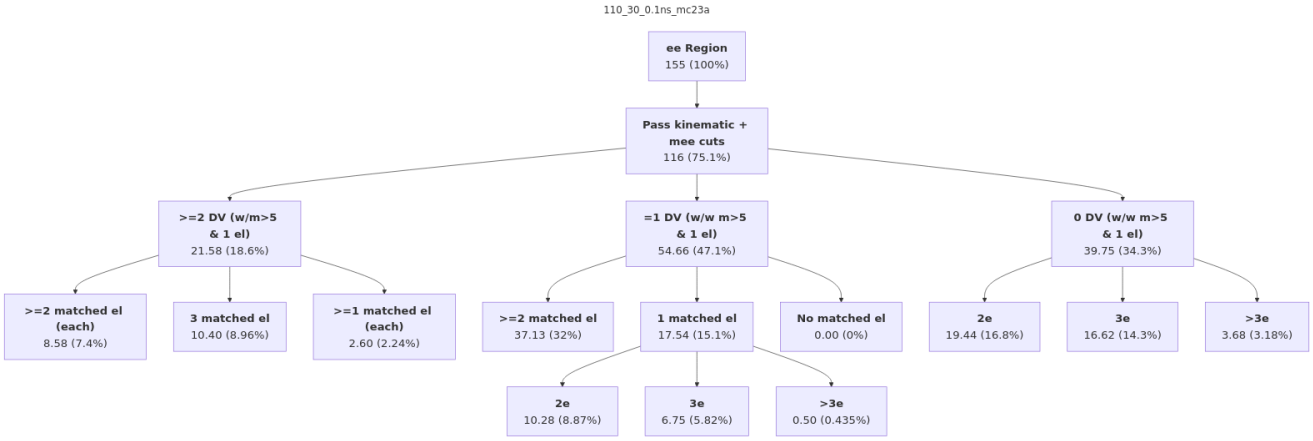

Figure 8: *A flowchart in the ee region showcasing the number and percentage of events passing each condition according to number of reconstructed DVs and number of matched electrons.*

The *ee* final state channel is not the only component of the search, however. The displacement of the final state electrons can also cause them to be mis-reconstructed as photons. To account for this, researchers at UT Austin are working on analyzing the $\gamma\gamma$ channel in which two photons are reconstructed instead of electrons, which becomes increasingly possible for longer lifetimes where larger displacements increase the likelihood of missing the charged tracks in the detector.

2.4 Mass Resolution Study

The work covered in this paper focuses on a mass resolution study in the *ee* channel of the long-lived dark photons search. The mass resolution of a sample is determined by plotting a histogram of reconstructed DV masses and fitting a gaussian to the resulting shape. The σ value of that gaussian is the sample's mass resolution. For this analysis an iterative gaussian approach was used in order to hone in on the core of the histogram's shape and ignore non-gaussian tails.

This meant iteratively fitting a gaussian until its σ value converged. Understanding how mass resolution behaves is crucial to the search, as a higher mass resolution represents how well the dark photon mass can be reconstructed, which in turn determines how well the signal can be discriminated from the background.

Since mZ_d, mS, and lifetime are parameters in HAHM, it is therefore important to study mass resolution across both masses and lifetimes. DV properties such as truth mass and displacement vary according to sample masses and lifetimes, so it is possible that the mass resolution may as well.

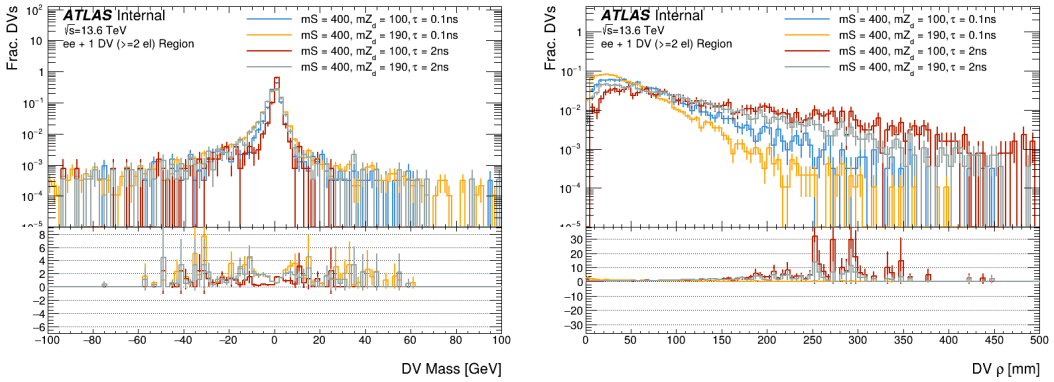

Figure 9: *Distributions of reconstructed DV mass (left) and DV displacement (right) for both 0.1 and 2 ns for $mZ_d = 100, mS = 400$ GeV and $mZ_d = 190, mS = 400$ GeV.*

2.4.1 2 Matched Leptons Case

The mass resolution study primarily puts emphasis on the case where each DV has two matched electrons, as this is the ideal case. The analysis used 68 Monte Carlo signal simulations consisting of 17 mass points with 4 lifetimes each. To start, mass histograms were constructed for each of these signal files, with iterative gaussians fit to them. This was done for each possible region of analysis, with those being events with at least two DVs per event, those with at least one, and those with exactly one.

In order to reduce the amount of resolution data points and variables the analysis needed to focus on, mass histogram distributions in each of these regions were plotted for each mass point, overlaying the histograms for all four of the mass point's lifetimes. These histograms were normalized to account for the fact that greater lifetimes saw less reconstructed DVs. There was no significant difference noticed in the resulting mass histograms between lifetimes, which justifies treating all four lifetimes for each mass point as one sample.

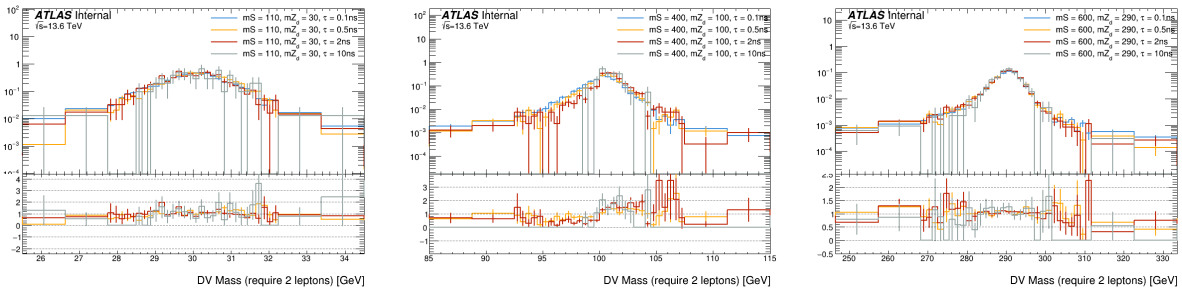

Figure 10: *Overlaid mass histogram distributions of all four lifetimes of $mZ_d = 30, mS = 110$ GeV (left), $mZ_d = 100, mS = 400$ GeV (center), and $mZ_d = 290, mS = 600$ GeV (right).*

The same process was then applied to the regions of interest. In events where only one DV is able to be reconstructed per event there is a higher risk of mismatching electrons, meaning an electron from one DV gets paired with an electron from another DV for the purpose of DV mass

reconstruction. For this reason it was possible that there would be a difference in mass resolutions between the one DV region and the region with at least two DVs per event where this was less likely. The mass histograms in both of these regions were plotted for each mass point, using the samples combining all four lifetimes. These histograms were again overlaid and normalized, again showing no significant difference between the two which justified focusing only on the combined region containing at least one DV per event.

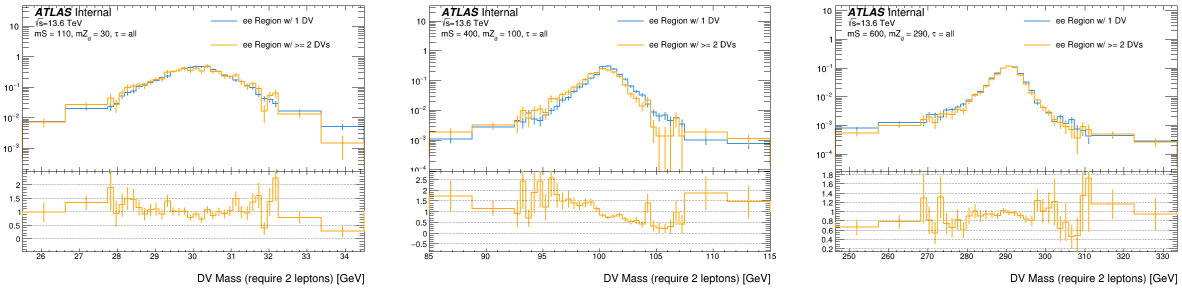

Figure 11: *Overlaid mass histogram distributions of both DV regions of* $mZ_d = 30, mS = 110$ *GeV (left),* $mZ_d = 100, mS = 400$ *GeV (center), and* $mZ_d = 290, mS = 600$ *GeV (right).*

With the combination of all lifetimes into one sample per mass point and of both regions into one of interest being justified, the resolution of these samples in this region could be analyzed. The mass histograms for each combined lifetime mass point were plotted in the region with at least one DV per event and a gaussian was iteratively fit to the core of each. Both the σ and μ values from these gaussians were then extracted to be analyzed.

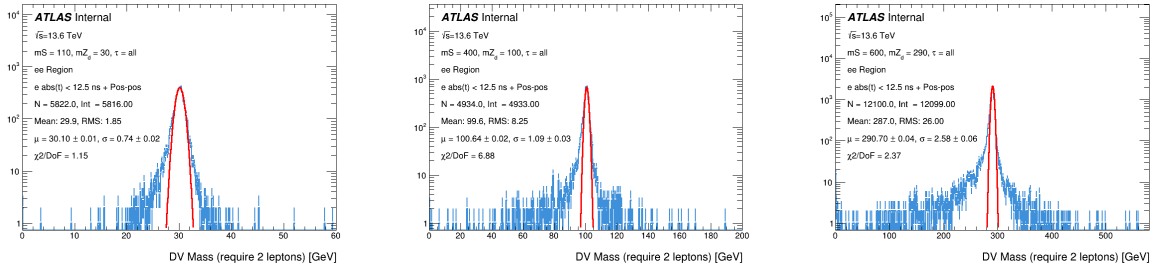

Figure 12: *Mass histograms with fitted gaussians in the* ≥ 1 *DV region for* $mZ_d = 30, mS = 110$ *GeV (left),* $mZ_d = 100, mS = 400$ *GeV (center), and* $mZ_d = 290, mS = 600$ *GeV (right).*

The resolution was plotted against both mZ_d and mS with fits being constructed and analyzed to observe trends. The resolution follows a linear trend against mZ_d with a slope of 0.1, and when plotted against both mZ_d and mS it increases against mass splitting (the ratio of mS to mZ_d) along a constant value of mZ_d, though to a lesser effect than against purely mZ_d. The effect of the mass splitting can explain the observed variation around the fit in the left plot of Figure 13, particularly for higher masses.

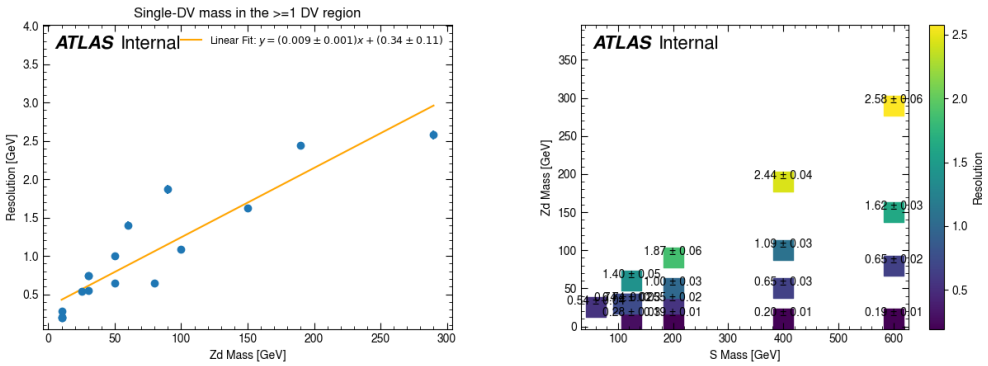

Figure 13: *Left: Reconstructed mass resolution plotted against mZd with a linear fit (orange). Right: Color-scale plot of reconstructed mass resolution against mS (x-axis) and mZ_d (y-axis).*

To further analyze how the dependence of the resolution on both mZ_d and mS, it was plotted against $mS - 2 \cdot mZ_d$. This was to account for the energy available for the dark photon to gain from the parent particle after the energy used to produce the two dark photons. The resolution follows a decreasing linear trend against $mS - 2 \cdot mZ_d$ with a slope of 0.0021. To further assess the validity of the fit, its residual was plotted, with values staying within $|1.5|$ GeV. Additionally, the resolution was plotted against both $mS - 2 \cdot mZ_d$ and mZ_d with a planar fit and the residuals were similarly plotted and remained less than $|0.5|$ GeV.

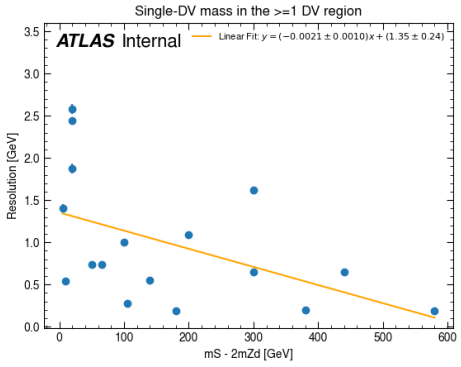

Figure 14: *Mass resolution plotted against $mS - 2 \cdot mZ_d$ with a linear fit (orange).*

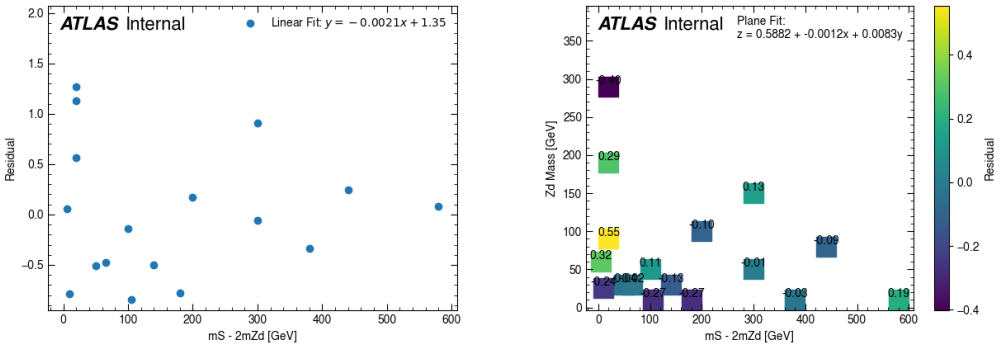

Figure 15: *Left: Residual of Figure 14 plotted against $mS - 2 \cdot mZ_d$. Right: Residual of a planar fit to resolution against $mS - 2 \cdot mZ_d$ and mZ_d*

Using the μ (mean) values extracted from the iterative gaussian fits of the mass histograms, these were plotted against mZ_d to ensure linearity. The trend of μ against mZ_d is linear with

a slope of 1 and offset of 0, which confirms there is no observed bias in the reconstructed mass versus the truth mass.

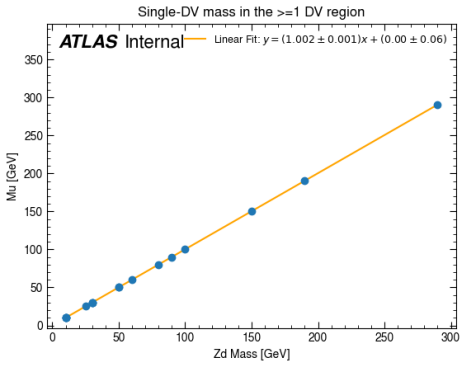

Figure 16: *Gaussian μ plotted against mZ_d.*

2.4.2 0 Matched Leptons Case

In the case where each DV has no matched electrons, the mass histograms were again plotted for each lifetime in each mass point, as well as across the regions of at least two, at least one, and exactly one DV per event. The histograms are non-gaussian and cannot have any fit made to them due to their poor shape, which confirms that it is not in the signal region of the analysis, as no signal can be reconstructed. This will further allow for plotting using data without the risk of accidental unblinding, as there is no signal to see.

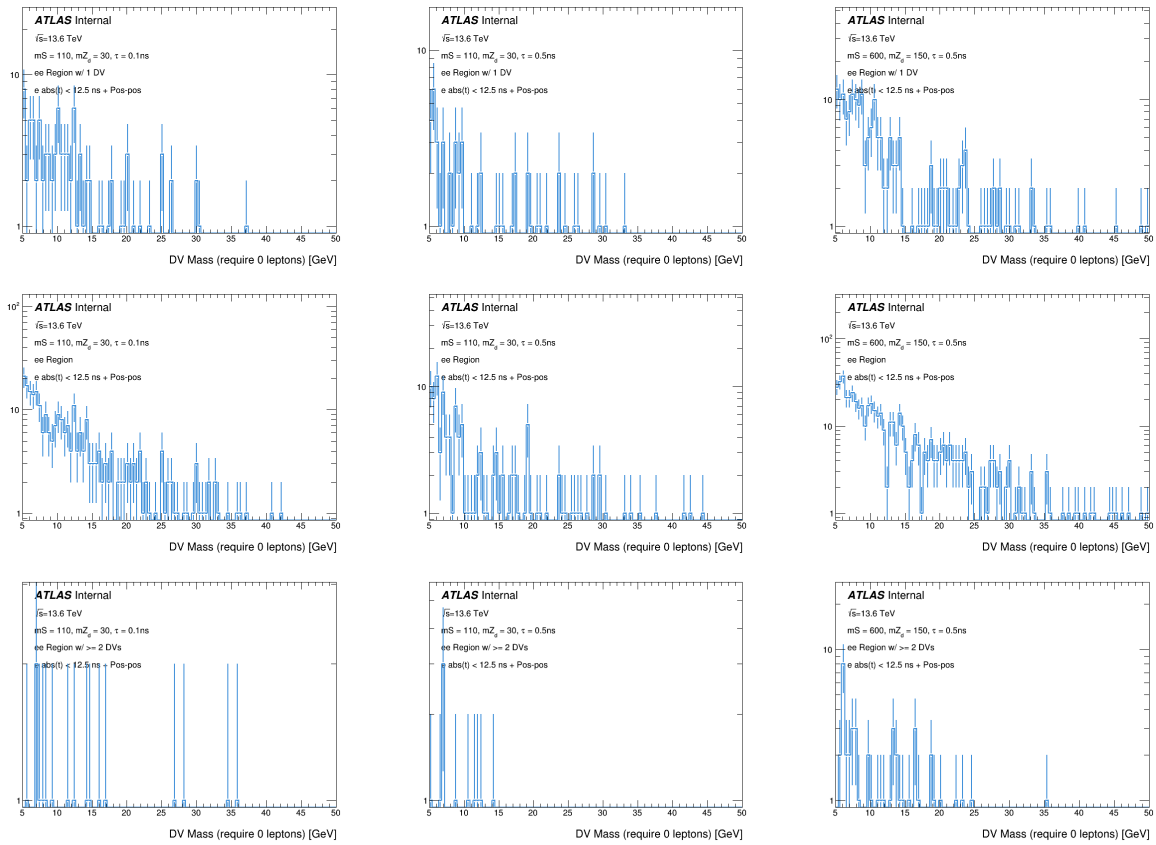

Figure 17: *Mass histograms in the case with no matched electrons per reconstructed DV. Left column: $mZ_d = 30, mS = 110$ GeV, $\tau = 0.1$ ns. Center column: $mZ_d = 30, mS = 110$ GeV, $\tau = 0.5$ ns. Right column: $mZ_d = 600, mS = 150$ GeV, $\tau = 0.5$ ns. Top row: Exactly 1 DV region. Middle row: ≥ 1 DV region. Bottom row: ≥ 2 DV region.*

In the region with at least two DVs per event, the DVs were sorted by mass and plotted separately. The distributions for the most massive DV as well as the second most were then overlaid to further analyze the behavior in this region, again showing nothing to reconstruct.

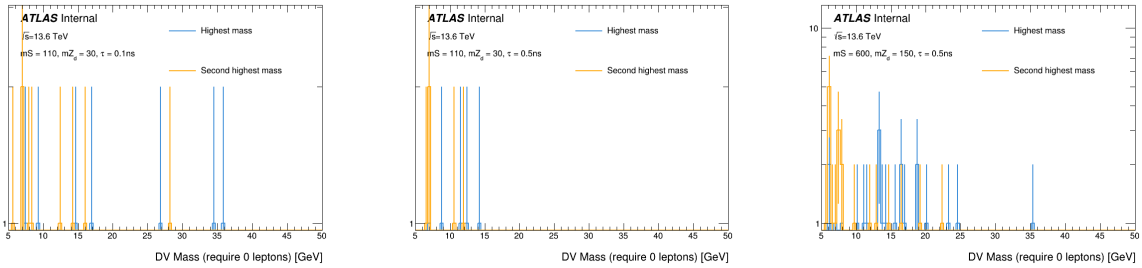

Figure 18: *Mass histograms in the ≥ 2 DV region of the case with no matched electrons per reconstructed DV with separate distributions for highest (blue) and second highest (orange) mass DVs. Left: $mZ_d = 30, mS = 110$ GeV, $\tau = 0.1$ ns. Center: $mZ_d = 30, mS = 110$ GeV, $\tau = 0.5$ ns. Right: $mZ_d = 600, mS = 150$ GeV, $\tau = 0.5$ ns.*

2.5 Conclusions and Future Work

The studies in the case of two DV-matched electrons for each DV show that the mass resolution is neither impacted by the lifetime of the signal, nor by the amount of DVs reconstructed per event. Moreover, they show that resolution increases linearly with mZ_d and along a constant mZ_d increases to a lesser effect against mass splitting. In the region with no DV-matched electrons in each DV, the shape demonstrates a lack of ability to reconstruct any signal, confirming that it is not the signal region, which allows for future analysis plotting data in that region without risk of accidental unblinding. Future analysis remains to be done in the region with one DV-matched electron in each DV.

3 Front End Board Upgrades for the ATLAS Liquid Argon Calorimeter

3.1 The High Luminosity LHC

In order to properly conduct effective searches for elusive BSM phenomena, an abundance of usable data is crucial. This amount of usable data is quantified by integrated luminosity $\mathcal{L}$ with units of inverse barns. For instantaneous luminosity L being the rate at which particles collide:

$$\mathcal{L} = \int L dt \tag{1}$$

During Run 2 of the LHC, ATLAS collected about 140 fb^{-1} of good data, but for future experiments and BSM searches, the integrated luminosity needs to be higher in order to set stricter limits on observed phenomena and to be able to study even more rare events than the LHC currently can [11]. For this reason, the LHC will soon be upgraded to the High Luminosity LHC (HL-LHC), which has been approved to run from 2030-2041 and is expected to deliver a total integrated luminosity of 3000 fb^{-1} by 2041 [12].

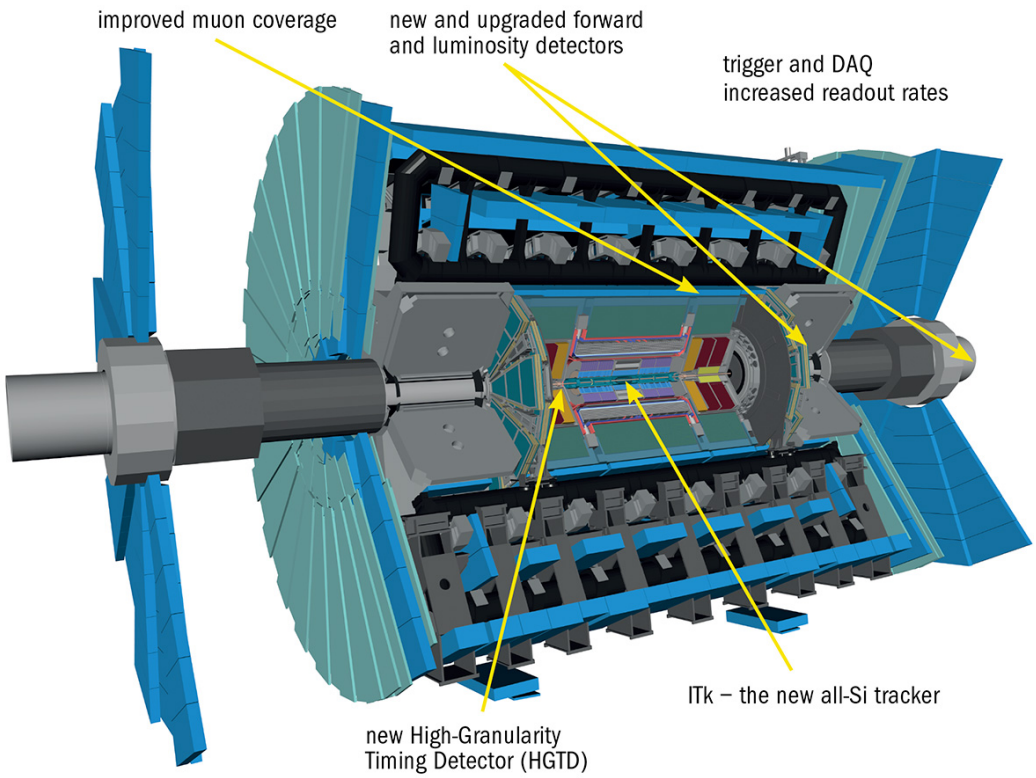

Figure 19: *The ATLAS detector for the HL-LHC [13].*

Of course to accommodate this increased luminosity, the ATLAS detector must also be upgraded so that it can handle and collect all the data passing through it. This upgrade is a massive undertaking which requires redesigns across all components of the detector, including the LAr calorimeter. As the LAr calorimeter works by measuring the currents produced by the ionization of liquid argon caused by the absorption of charged particles, the electronics which handle and interpret these currents must be able to manage the increase in currents produced by the HL-LHC. One crucial component of these electronics is the front end board (FEB), which the Columbia ATLAS group is working to develop the upgrade for.

3.2 The Front End Board 2

The job of the front end board is to take the currents from the liquid argon and convert it into a digital signal that can be read. The upgraded front end board for the HL-LHC (FEB2) will have to be able to handle even more currents than the current iteration. To achieve this, 1524 boards will be used by the detector, each with 128 calorimeter channels. The board works by first sending the input through LAUROC preamplifier chips to amplify the signal before being digitized by COLUTA analog-to-digital (ADC) ASIC chips. The digitized signal is then serialized by lpGPT chips and sent out of the board.

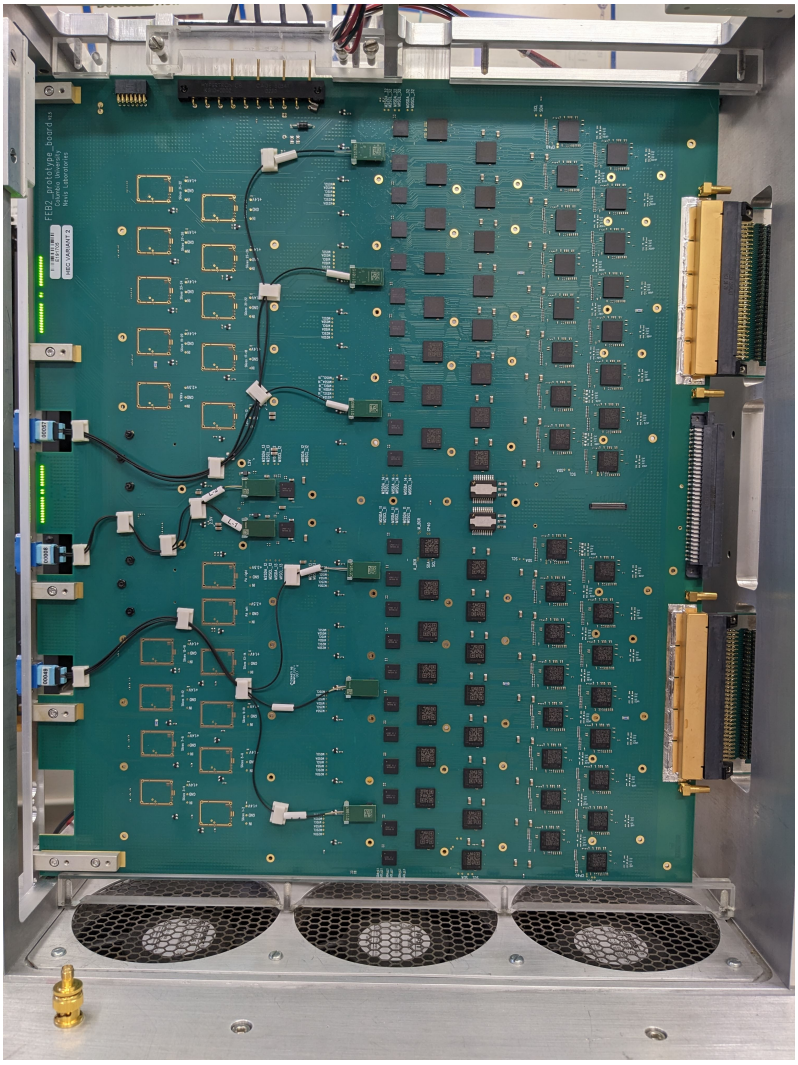

Figure 20: *An example FEB2.*

The FEB2 design is nearly complete and ready to enter mass production and quality control testing (QC), but first some preparations for QC need to be completed. This includes having a system which can determine if the COLUTA ADC ASIC chips are sufficiently uniform and outputting correct signals.

3.2.1 COLUTA ADC ASIC Calibration Constants

To ensure only satisfactory COLUTA chips are used in the final boards, their "calibration constants" are analyzed. The constants are how the chip is able to convert an input voltage into binary to digitize it.

If efficiency were not a consideration, decreasing powers of 2 known as "binary weights" can be used to convert a voltage into binary. If the weights used are 8, 4, 2, and 1 (which would output a 4-digit binary number), then an algorithm first checks if the voltage is above or below 8. If it's above, then the first digit is 1 and if it's below the first digit is 0. It then checks to see if the voltage is above or below 4 plus the product of the first digit and 8. Again, above assigns a 1 to the second digit and below assigns a 0. This process is continued until each binary digit is constructed corresponding to the voltage.

However, in the interest of efficiency the COLUTA chips instead us non-binary weights. This is because in the algorithm described, there is only one path through which binary weights can reach the correct voltage and if a mistake is made then the final output is also incorrect. Non-binary weights, on the other hand, can take multiple paths to get to the same value. This means

that if a wrong decision is made in this process like assigning a 1 instead of a 0, which can happen if the chip is trying to execute this process very fast, it can be corrected later and still reach the right output. These binary weights are called the COLUTA "calibration constants".

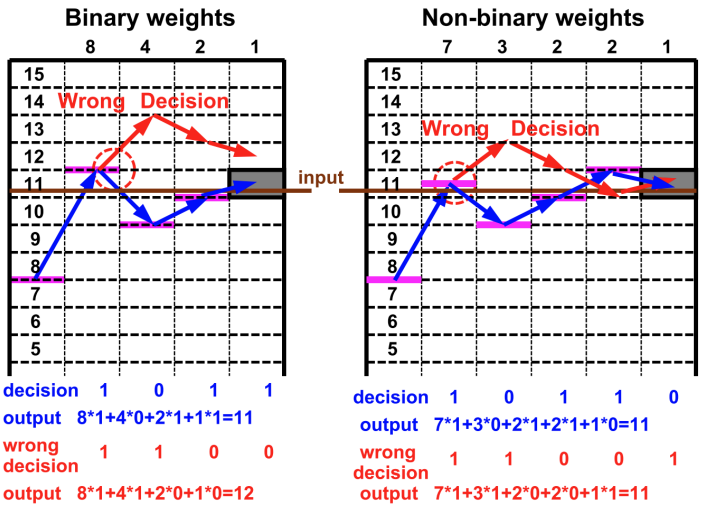

Figure 21: *Model of how binary weights (left) can only get to a value one way whereas non-binary weights (right) can correct for mistakes [14].*

Ideally these constants would be the same across all chips and all channels within each chip. However, the capacitors which determine each channel's calibration constants are imperfect, which in turn leads to fluctuations in the values of the calibration constants. Therefore it is important to determine that all constants across all implemented chips are within an acceptably small range of each other.

The chips are produced at UT Austin and Saclay where they are robotically tested standalone to sort out any chips with channels that have constants more than 20% away from the mean. In addition, the calibration constants for each channel come in two types: "mdac" and "sar", with sar constant values being subject to a scaling factor.

3.3 Outlier Search and Analysis of Calibration Constants

At Columbia with the chips soldered into the boards it becomes important to cross check these constants to again ensure that they are within an acceptable range, as well as to develop criteria for such acceptable ranges which can be used in future QC testing. To begin this analysis, histograms were plotted for each calibration constant to observe the shape of the values across boards. The distributions are roughly gaussian for mdac constants, however significant non-gaussian outliers appear in the sar histograms when the scaling factors are not applied. When the scaling factors were applied to the sar constants, the distribution became far narrower and the outliers compressed, causing the distribution to appear more gaussian like the plots for the mdac constants.

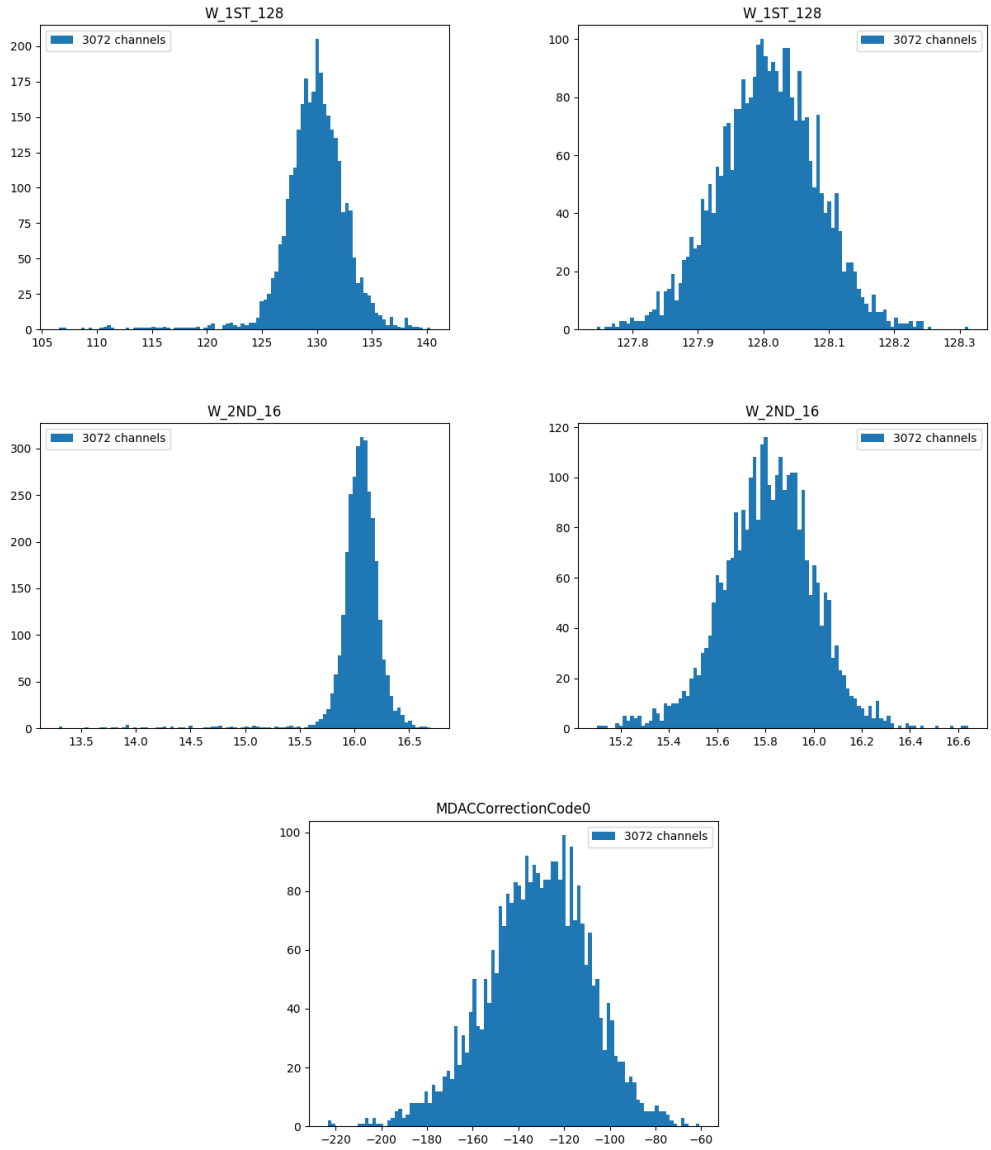

Figure 22: *Histograms for W_1ST_128 unscaled (top left) and scaled (top right), W_2ND_16 unscaled (middle left) and scaled (middle right), and MDACCorrectionCode0 (bottom) with units of ADC counts.*

To further investigate the behavior of outliers, particularly in relation to the scaling process, the channels were sorted to identify any which had at least one unscaled calibration constant value which was an outlier in that constant's histogram. These outliers were defined as being $\pm 5\sigma$ away from the mean of that calibration constant's distribution. Histograms were then produced to plot the difference between these unscaled outlier calibration constant values and their respective means. Notably, several of the plots produced had nearly identical shapes, with many channels having their outliers appear in the same set of constants as each other with very similar values plotted for each.

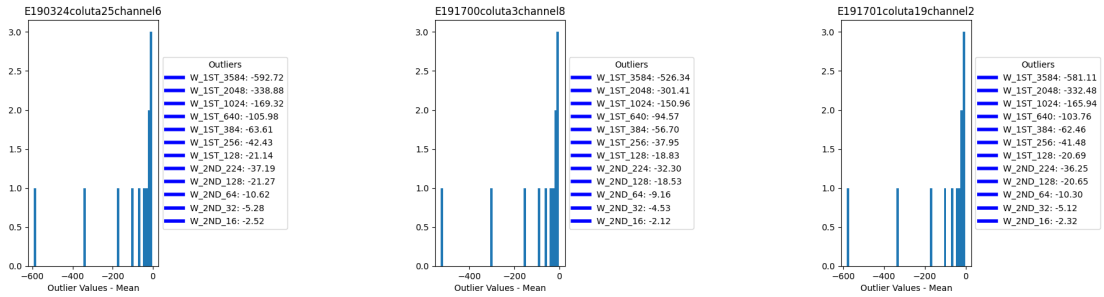

Figure 23: *Histograms of unscaled outlier values minus the means of their respective distributions for board E190324 chip coluta25 channel 6 (left), board E191700 chip coluta3 channel 8 (center), and board E191701 chip coluta19 channel 2 (right) with units of ADC counts.*

As the majority of these outliers were identified in sar constants, the next step was to examine the effect of the the scaling factors on the outliers in these distributions. Similar histograms were produced which only plotted values which were outliers while unscaled, but applied the scaling factors before plotting. Upon scaling the values which were unscaled outliers, there was no longer a pattern among the shapes of the distributions, and the differences between the values and the means decreased significantly, making it so that the values which were outliers while unscaled were no longer outliers and now very close to the center of the distribution.

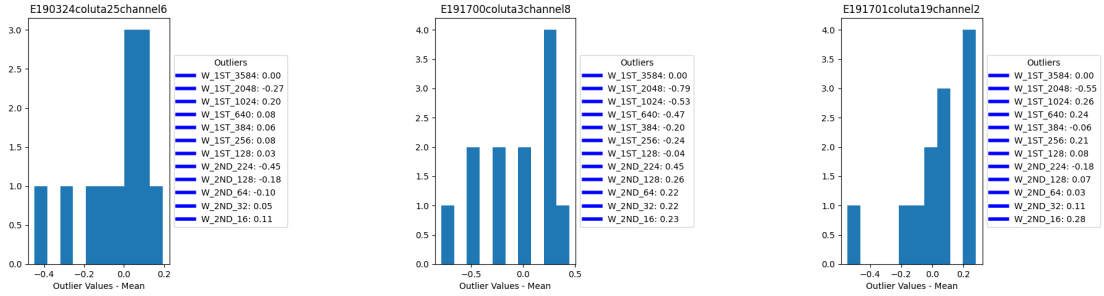

Figure 24: *Histograms of scaled values minus the means of the respective distributions of the outliers in Figure 23 for board E190324 chip coluta25 channel 6 (left), board E191700 chip coluta3 channel 8 (center), and board E191701 chip coluta19 channel 2 (right) with units of ADC counts.*

3.4 Conclusions and Future Work

The analysis of the COLUTA calibration constants and their outliers shows that the sorting performed robotically at UT Austin and Saclay for chips with constants within 20% of the mean, as well as the scaling performed on the sar constants successfully keeps these values within an acceptable range for chips implemented into the FEB2 boards. The boards will soon go into mass production, during which this understanding of the distributions of calibration constants will prove useful for the quality control tests performed on the newly produced boards. The quality control process will in part be used to determine if the values for all chips are within an acceptable range before approving them for use in the upgraded ATLAS detector for the HL-LHC.

4 Acknowledgments

Thank you to everyone who made this year's Nevis Labs REU possible, including Professor John Parsons, Professor Georgia Karagiorgi, Professor Reshmi Mukherjee, and Amy Garwood. A special thank you to Eleanor Woodward, Dr. Daniel Williams, Dr. Jonathan Long, and Dr. Lauren Osojnak for guiding me and my work throughout this process. Lastly, thank you to the

entire Columbia ATLAS Group and all other participants in this year's REU for cultivating a welcoming and memorable Summer.

This material is based upon work supported by the National Science Foundation under Grant No. PHY-2349438.

References

[1] CERN. The standard model, n.d. Accessed: 2025-07-29.

[2] U.S. Department of Energy. Doe explains... the standard model of particle physics, n.d. Accessed: 2025-07-29.

[3] CERN. Dark matter, n.d. Accessed: 2025-07-29.

[4] CERN. Accelerators, n.d. Accessed: 2025-07-29.

[5] CERN. Accelerator complex panoramas, n.d. Accessed: 2025-07-29.

[6] ATLAS Collaboration. Atlas experiment overview, n.d. Accessed: 2025-07-29.

[7] ATLAS Collaboration. Atlas calorimeter, n.d. Accessed: 2025-07-29.

[8] ATLAS Collaboration. Atlas detector overview, n.d. Accessed: 2025-07-29.

[9] David Curtin, Rouven Essig, Stefania Gori, and Jessie Shelton. Illuminating dark photons with high-energy colliders. *Journal of High Energy Physics*, 2015(2), February 2015.

[10] ATLAS Collaboration. Search for a new scalar decaying into new spin-1 bosons in four-lepton final states with the atlas detector. *Physics Letters B*, 865:139472, June 2025.

[11] ATLAS Collaboration. Atlas measures run-2 luminosity, 2021. Accessed: 2025-07-29.

[12] ATLAS Collaboration. Atlas prepares for the high-luminosity lhc, n.d. Accessed: 2025-07-29.

[13] CERN Courier. A new atlas for the high-luminosity era, 2023. Accessed: 2025-07-29.

[14] Wei-Hsin Tseng, Wei-Liang Lee, Chang-Yang Huang, and Pao-Cheng Chiu. A 12-bit 104 ms/s sar adc in 28 nm cmos for digitally-assisted wireless transmitters. *IEEE Journal of Solid-State Circuits*, 51(10):2222–2231, 2016.